Draft version February 1, 2008
Preprint typeset using LaTeX style emulateapj v. 10/09/06

WHY DO SOME INTERMEDIATE POLARS SHOW SOFT X-RAY EMISSION? A SURVEY OF *XMM-Newton* SPECTRA.

P.A. Evans[1] and Coel Hellier
Astrophysics Group, Keele University, Staffordshire, ST5 5BG, UK
Draft version February 1, 2008

ABSTRACT

We make a systematic analysis of the *XMM-Newton* X-ray spectra of intermediate polars (IPs) and find that, contrary to the traditional picture, most show a soft blackbody component. We compare the results with those from AM Her stars and deduce that the blackbody emission arises from reprocessing of hard X-rays, rather than from the blobby accretion sometimes seen in AM Hers. Whether an IP shows a blackbody component appears to depend primarily on geometric factors: a blackbody is not seen in those that have accretion footprints that are always obscured by accretion curtains or are only visible when foreshortened on the white-dwarf limb. Thus we argue against previous suggestions that the blackbody emission characterises a separate sub-group of IPs which are more akin to AM Hers, and develop a unified picture of the blackbody emission in these stars.

Subject headings: accretion, accretion discs – novae, cataclysmic variables – X-rays: binaries.

1. INTRODUCTION

Intermediate polars (IPs) – interacting binaries with a magnetic white-dwarf primary – have traditionally been noted for their hard X-ray emission. This arises as the magnetic field of the white dwarf disrupts the accretion disc and channels material towards the magnetic polecaps. This material forms stand-off shocks, below which it cools via free-free interactions, producing hard X-rays. However, a growing number of systems have been shown to emit a distinct blackbody component in softer X-rays (e.g. Mason et al. (1992); Haberl et al. (1994); de Martino et al. (2004)), reminiscent of the soft component prominent in the X-ray spectra of many AM Her stars (also known as polars). These systems are similar to IPs but the white-dwarf has a magnetic field strong enough to prevent an accretion disc from forming at all. In these systems, the soft blackbody component is though to arise from a heated polecap surrounding the accretion column (See Warner (1985); Hellier (2001) for a review of these objects).

Currently it is unclear why the blackbody component is seen in some IPs and not others. Haberl & Motch (1995) suggested that there are two distinct classes of IP, with the 'soft' systems being evolutionary progenitors of polars. They argued that the 'hard IPs' may have larger and cooler polecaps, pushing the soft emission into the EUV and explaining the difference in the spectra.

We present here a study of *XMM-Newton* X-ray data of 12 IPs, aimed at discovering why some IPs show a blackbody component while others don't. Our method is similar to that of Ramsay & Cropper (2004) (hereafter RC04) who analysed the *XMM-Newton* data of twenty-one polars, which enables us to compare the IPs with the polars.

2. OBSERVATIONS AND DATA ANALYSIS

The *XMM-Newton* observatory (Jansen et al. 2001) was launched in 1999, and we have obtained observations of twelve IPs from the public archive. We analyzed the data from the EPIC-MOS and pn instruments (Turner et al. 2001; Strüder et al. 2001) which provide high-throughput, medium-resolution spectroscopy across the 0.2–12 keV energy range. The higher resolution RGS instruments (den Herder et al. 2001) have only 20 per cent of the effective area of the MOS cameras and the data are not used here.

TABLE 1
The *XMM* observations of IPs analysed in this paper.

Object	ObsID	Date	References
AO Psc	0009650101	2001-06-09	1,2
EX Hya	0111020101	2000-07-01	1,2
	0111020201	2000-07-01	1,2
FO Aqr	0009650201	2001-05-12	1,2,3
GK Per	0154550101	2002-03-09	2,4
HT Cam	0144840101	2003-03-24	2,5,6
PQ Gem	0109510301	2002-10-08	2,7
NY Lup	0105460301	2000-09-07	2,8
UU Col	0201290201	2004-08-21	9
V1223 Sgr	0145050101	2003-04-13	1,2
V405 Aur	0111180401	2001-10-05	2,10
V2400 Oph	0105460601	2001-08-30	2
WX Pyx	0149160201	2003-05-20	11

References. — (1) Cropper et al. (2002), (2) Evans & Hellier (2005b), (3) Evans et al. (2004), (4) Vrielmann et al. (2005) (5) de Martino et al. (2005), (6) Evans & Hellier (2005a), (7) Evans, Hellier & Ramsay (2006), (8) Haberl et al. (2002), (9) de Martino et al. (2006) (10) Evans & Hellier (2004), (11) Schlegel (2005).

A summary of the observations used is given in Table 1. We re-ran the pipeline processing for these observations using XMM-SAS v7.0.0. The observations of GK Per, NY Lup and V2400 Oph suffered from pile-up, and thus only the wings of the PSF were included in the source extraction. The MOS-1 observation of EX Hya was so badly piled up that we excluded it from our analysis.

RC04 used only the EPIC-pn data as it was better calibrated than the EPIC-MOS data at soft energies. Using the better calibrations of XMM-SAS v.7 we extracted

[1] Current address: Department of Physics and Astronomy, University of Leicester, Leicester, LE1 7RH, UK

spectra from all three EPIC instruments. Response matrices were created for each spectrum, using the XMM-SAS rmfgen and arfgen tasks. We then modelled the spectra using XSPEC V11. For each star, all model parameters were tied between the EPIC instruments, except for the normalisation which we allowed to vary in order to combat the effects of cross-calibration uncertainties.

Although IP spectra can vary considerably over the spin cycle, for the majority of the systems in this paper, we do not have enough geometric information to identify phase regions when the hard/soft components are best presented to us (as RC04 did), so we extracted spectra covering the entire observation. Note that the results of our spectroscopy are thus weighted averages from across the spin cycle; this was taken into account when interpreting our results .

To reproduce the hard component we used the stratified accretion column model of Cropper et al. (1999). This models the spectrum in terms of the white dwarf mass ($M_{\rm WD}$) and specific accretion rate (i.e. accretion rate per unit area, $\dot{m}$), from which it calculates the temperature and density profile of the column. This is then divided into 100 bins, evenly distributed in velocity space, each bin emitting as an optically thin plasma (a MEKAL). To the stratified column model, we added narrow Gaussians for the 6.4-keV iron fluorescence line and the 0.547 keV Oxygen VII photoionisation line where necessary. We then applied to this emission a simple photoelectric absorber. For most systems this did not give an acceptable fit, so we added either one or two partial-covering absorbers as necessary.

Next, we added a blackbody component to the models. Since absorption at the densities of the partial-covering components (typically $\sim 10^{23}$ cm^{-2}) will completely smother any soft X-ray emission and thus be redundant with model normalisation, the blackbody component was absorbed only by the simple absorption, which was of order 10^{19}–10^{21} cm^{-2}.

For some systems the addition of a blackbody did not improve the fit. For these systems we manually raised the blackbody normalisation until it significantly reduced the fit quality, thus finding an upper limit. Since this will be temperature dependent, we did this for blackbody temperatures of 40, 60 and 80 eV.

We quote, in Table 2, the f-test statistic to judge the the significance of adding the blackbody component. However, this test will produce false positives in the presence of calibration systematics. We have thus estimated the systematics by fitting a model optimised for the MOS data to the pn data (allowing only the normalisation to change) and recording the change in $\chi^2 (=\Delta\chi^2_{\rm system})$. We claim the presence of a blackbody only if it improves the χ^2 by more than $\Delta\chi^2_{\rm system}$. This method is more conservative than using the f-test alone. We include this estimate of the systematics in all the errors quoted in this paper.

Details of the fits are given in Table 3. The $\dot{m}$ was unconstrained for every system, so is not given. We do not quote errors on the partial-covering absorbers as they do not affect the softness ratio. The ratio is sensitive, however, to the metal abundance in the column, as there is a forest of iron L lines in the 0.5–1.2 keV range, affecting the model fit at the soft end.

For all twelve systems we then calculated the flux from the hard and soft components. Following RC04 we defined the softness ratio as $F_s/4F_h$, where F_s and F_h are the fluxes of the soft and hard components respectively. The factor of four arises because the hard component is optically thin and thus radiates isotropically, whereas the hard component is optically thick. Where the blackbody-emitting region is seen foreshortened, the observed ratio will be an underestimate.

The softness ratios are shown in Figs. 1 and 2. We show the observed ratio, the ratio of unabsorbed fluxes over the 0.2–12 keV range, and the ratio of unabsorbed fluxes calculated over all energies. These bolometric fluxes and softness ratios are given in Table 4. For the systems with no detectable soft component we show the upper limit calculated for a 60-eV blackbody, and present the fluxes and ratios for a range of blackbody temperatures in Table **??**.

3. RESULTS

We show the spectra for the systems with a blackbody component in Fig. 3, and for those without in Fig. 4. For the latter we have also shown the upper limit determined for a 60-eV blackbody component.

For FO Aqr, AO Psc, V1223 Sgr and HT Cam we found no evidence for a soft component, in agreement with previous observations, (see Norton et al. (1992); Hellier et al. (1996); Beardmore et al (2000); Evans & Hellier (2005a) respectively).

3.1. *V405 Aur*

The *XMM* observation of V405 Aur contains systematic discrepancies between the two EPIC-MOS instruments below 0.4 keV. However, when processed under SAS 7.0 these are at a much lower level than when Evans & Hellier (2004) analysed the data, and we have made no allowance for these discrepancies in the fit. Note also that as there is no pn data for V405 Aur, we have no estimate of the effects of systematics discussed in Section 2, so our errors are likely to be underestimates.

The best-fitting blackbody temperature was $kT = 64.78^{+0.81}_{-1.11}$ eV. This is significantly higher than the 40 ± 4 eV reported by Evans & Hellier (2004) analysing the same observation, however they used two MEKALs to fit the hard component whereas we used the stratified column model. Since the calibration has also changed since Evans & Hellier (2004), we analysed our better-calibrated data using their model, and found a fit in agreement with theirs. This demonstrates that the results are somewhat model dependent; the stratified column model is likely to be the more physically realistic. Fitting the hard component with a single, high temperature plasma, Haberl et al. (1994) found a blackbody temperature of 49–64 eV (from *ROSAT* data) and de Martino et al. (2004) found 73 ± 14 eV (using *BeppoSAX*).

Our fitted hydrogen column of $3.46^{+0.41}_{-0.31} \times 10^{20}$ cm^{-2} agrees with that of de Martino et al. (2004) [$(4\pm2)\times10^{20}$ cm^{-2}] but not with those of Haberl et al. (1994) or Evans & Hellier (2004) who reported $(5.7 \pm 0.3) \times 10^{20}$ and $(10.6^{+0.9}_{-1.2}) \times 10^{20}$ cm^{-2} respectively. However, the fitted column will depend on the emission model used, so some discrepancy is expected.

TABLE 2
FIT STATISTICS FOR EACH STAR WITH AND WITHOUT A BLACKBODY.

Star	χ^2 (dof) (No bb)	χ^2 (dof) (with bb) (with bb)	f-test	$\Delta\chi^2_{\rm system}$	$\chi^2_{\rm nobb} - \chi^2_{\rm bb}$
AO Psc	3372.74 (2888)	3772.71 (2884)	0.93	700	0.03
FO Aqr	1462 (1864)	1444 (1860)	1.6×10^{-4}	168	18
HT Cam	1325 (1273)	1310 (1269)	4.1×10^{-3}	79	16
V1223 Sgr	3840.8 (3128)	3840.6 (3124)	0.99	143	0.2
EX Hya	14045 (4876)	10158 (4873)	$< 10^{-99}$	1284	3887
GK Per	17040 (4079)	5024 (4075)	$< 10^{-99}$	84	12016
NY Lup	902 (699)	669 (695)	8×10^{-14}	40	233
PQ Gem	20435 (2439)	2940 (2435)	$< 10^{-99}$	144	17495
UU Col	1676 (817)	910 (813)	$< 10^{-99}$	76	766
V2400 Oph	1019 (1003)	953 (999)	9×10^{-14}	50	66.15
V405 Aur	17626 (997)	1146 (994)	$< 10^{-99}$	*	16480
WX Pyx	594 (477)	495 (473)	8×10^{-18}	52	99

NOTE. — The f-test gives the probability that no blackbody is present, making no allowance for systematics. The $\Delta\chi^2_{\rm system}$ is the change in χ^2 in fitting the same model to the MOS and pn cameras, thus giving an estimate of the systematic errors. The last column is the improvement in χ^2 when a blackbody is added. We consider this significant if it exceeds $\Delta\chi^2_{\rm system}$. * There was no pn data for V405 Aur, so $\Delta\chi^2_{\rm system}$ was not estimated.

TABLE 3
SPECTRAL COMPONENTS USED IN THE FITTED MODELS.

Star	wabs n_H (10^{20}cm^{-2})	blackbody kT (eV)	Part Abs (1) (n_H, Cv Frc)	Part Abs (2) (n_H, Cv Frc)	$M_{\rm WD}$ ($M_\odot$)	Abundance (solar)
V405 Aur	3.46 (+0.41, −0.31)	64.78 (+0.81, −1.11)	17, 0.49	3.0, 0.63	0.40 (+0.05, −0.06)	0.069 (+0.024, −0.021)
GK Per	23.3 (+2.0, −1.9)	62 (±2)	23, 0.74	4.7, 0.45	0.92 (+0.39, −0.13)	0.21 (+0.14, −0.07)
NY Lup	7.8 (±3.9)	104 (+21, −23)	14, 0.49	0.38, 0.71	0.96 (+0.40, −0.55)	0.68 (+0.51, −0.59)
V2400 Oph	7.0 (+2.9, −4.9)	117 (+33, −44)	11, 0.52	0.61, 0.53	0.69 (+0.06, −0.24)	0.33 (+0.12, −0.10)
PQ Gem	0 (+0.30)	47.6 (+2.9, −1.4)	42, 0.60	3.4, 0.56	0.70 (+0.16, −0.14)	< 0.08
EX Hya	9.76 (+2.2, −0.86)	31.0 (+1.3, -2.4)	75, 0.35	4.0, 0.29	0.449 (+0.005, −0.013)	0.514 (+0.01, −0.0029)
UU Col	0 (+0.59)	73 (+20, −9)	10, 0.34		1.23 (+0.17, −0.29)	0.66 (+1.0, -0.62)
WX Pyx	8.4 (+3.8, −2.9)	82 (+11, −15)			1.4 (+0, −0.09)	< 2.87
FO Aqr	0 (+2.1)		21, 0.80	6.4, 0.98	1.19 (+0.11, −0.31)	0.31 (+0.20, −0.23)
AO Psc	3.89 (+0.69, −1.44)		14, 0.62	1.8, 0.75	0.594 (+0.13, −0.040)	0.362 (+0.20, −0.064)
HT Cam	3.86 (+0.81, -0.88)				0.687 (+0.094, −0.061)	0.52 (+0.24, −0.11)
V1223 Sgr	1.03 (+0.36, −0.52)		13, 0.46	1.3, 0.63	1.046 (+0.049, −0.012)	0.398 (+0.090, -0.049)

NOTE. — The column density of the partial absorption is given in units of 10^{22} cm^{-2}. Errors are quoted to the same power of ten as the corresponding parameter.

TABLE 4
THE UNABSORBED, BOLOMETRIC FLUXES OF THE SOFT AND HARD COMPONENTS FOR THOSE SYSTEMS WHICH SHOW BLACKBODY EMISSION.

Object	$F_{h,\rm bol}$ (erg s^{-1} cm^{-2})	$F_{s,\rm bol}$ (erg s^{-1} cm^{-2})	Ratio
V405 Aur	5.1×10^{-11} (+3.6, −1.1)	4.3×10^{-11} (+2.4, −1.2)	0.211 (+0.018, -0.038)
GK Per	1.20×10^{-9} (+0.25, −0.06)	2.29×10^{-10} (+0.95, −0.62)	4.8×10^{-2} (+1.8, −1.3)
NY Lup	4.15×10^{-11} (+12.7, −0.18)	4.3×10^{-12} (+9.9, −1.4)	2.6×10^{-2} (+1.6, −1.1)
V2400 Oph	9.2×10^{-11} (+4.1, −1.9)	3.3×10^{-12} (+2.1, −1.5)	8.9×10^{-3} (+4.6, −2.8)
PQ Gem	1.07×10^{-10} (+0.40, −0.23)	1.33×10^{-11} (+0.13, −0.17)	3.11×10^{-2} (+0.74, −0.83)
EX Hya	3.95×10^{-10} (+0.26, −0.20)	1.59×10^{-10} (+3.47, −0.62)	1.00 (+0.48, −0.20)
WX Pyx	7.51×10^{-12} (+0.35, −0.93)	6.0×10^{-13} (+5.9, −2.9)	2.00×10^{-2} (+2.38, −0.93)
UU Col	6.81×10^{-12} (+2.29, −0.80)	3.04×10^{-13} (±0.98)	1.12×10^{-2} (±0.45)

NOTE. — The ratio is defined as in Fig. 1. Errors are given to the same power of ten as the values.

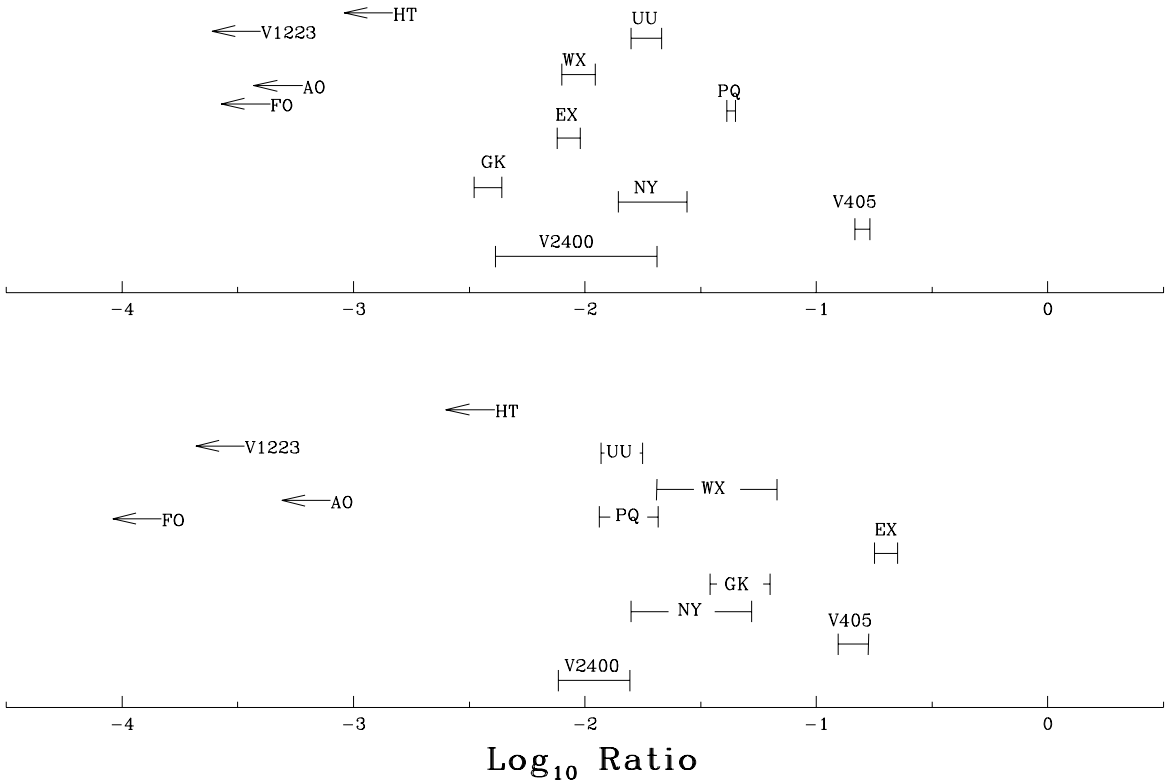

FIG. 1.— Softness ratios of the IPs observed with *XMM*, defined as $F_s/4F_h$, where F_s and F_h are the fluxes of the soft blackbody and hard plasma components respectively, calculated over the 0.2–12 keV energy range covered by *XMM*. *Upper panel*: Ratios calculated from the spectral fits. *Lower panel*: The ratios calculated from the spectral fits, after the absorption components were removed.

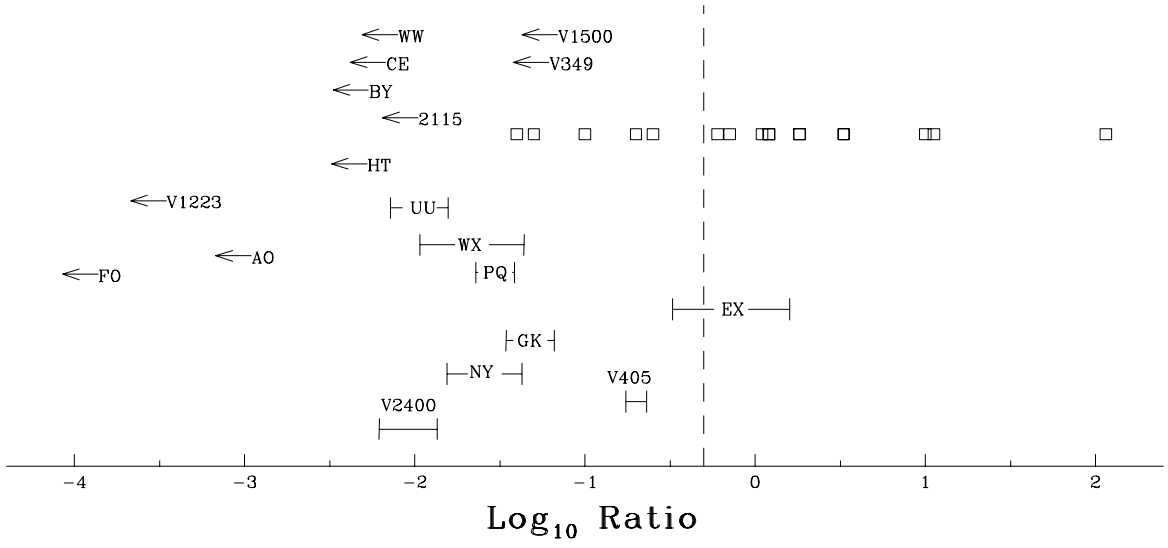

FIG. 2.— As for Fig. 1, but with the effects of absorption removed and F_s and F_h extended over all energies. The ratios for the polars given in RC04 are also shown (hollow squares); RC04 did not quote errors. The uppermost six systems are the polars in which RC04 found no blackbody component. We have found an upper limit for these systems as we did for the IPs. The dashed line corresponds to a softness ratio of 0.5; systems with a higher softness ratio exhibit a 'soft excess'.

TABLE 5
The unabsorbed, bolometric fluxes from the systems with no detectable soft X-ray component, and the upper limit of the softness ratio, for a range of temperatures.

Object	$F_{h,\rm bol}$	$\rm Ratio_{40eV}$ (erg s^{-1} cm^{-2})	$\rm Ratio_{60eV}$	$\rm Ratio_{80eV}$
FO Aqr	$2.71 \times 10^{-10}(+0.65, -0.18)$	$< 4.6 \times 10^{-4}$	$< 1.4 \times 10^{-4}$	$< 8.0 \times 10^{-5}$
AO Psc	$1.51 \times 10^{-10}(+0.09, -0.11)$	$< 4.3 \times 10^{-3}$	$< 1.1 \times 10^{-3}$	$< 6.2 \times 10^{-4}$
HT Cam	$8.48 \times 10^{-12}(+0.53, -0.38)$	$< 2.5 \times 10^{-2}$	$< 5.3 \times 10^{-3}$	$< 2.6 \times 10^{-3}$
V1223 Sgr	$2.96 \times 10^{-10}(\pm 0.13)$	$< 8.5 \times 10^{-4}$	$< 3.5 \times 10^{-4}$	$< 2.3 \times 10^{-4}$

3.2. *GK Per*

A soft blackbody component was necessary to model the *XMM* spectrum of GK Per as previously found by Vrielmann et al. (2005). They reported a blackbody temperature of 59.6 ± 0.2 eV absorbed by a column of $(3.2 \pm 0.2) \times 10^{21}$ cm^{-2}. Our temperature of 62 ± 2 eV and column of (2.3 ± 0.2) cm^{-2} are very similar, though not formally in agreement. Note that Vrielmann et al. (2005) parameterised the hard emission using a bremsstrahlung component and a MEKAL, supporting our assertion above that these results are model dependent.

3.3. *NY Lup*

Haberl et al. (2002) analysed this *XMM* observation of NY Lup (=RX J154814) and found a soft component with a blackbody temperature of 84–97 eV and a column density of (11.7–15.5) $\times 10^{20}$ cm^{-2}. Our values of $kT_{\rm bb} = 104^{+21}_{-23}$ eV and $n_H = (7.8 \pm 3.9) \times 10^{21}$ cm^{-2} agree.

3.4. *V2400 Oph*

V2400 Oph was identified as a soft IP by de Martino et al. (2004), who analysed a *BeppoSAX* observation and reported a blackbody temperature of 103 ± 10 eV and absorption column $(46^{+12}_{-13}) \times 10^{20}$ cm^{-2}. We find a blackbody temperature of 117^{+33}_{-44} eV, in agreement with this result, but a slightly lower absorption column of $(7.0^{+2.9}_{-4.9}) \times 10^{20}$ cm^{-2}. This is probably because de Martino used a single MEKAL and a single partial-covering absorber to model the hard emission, whereas we used the stratified column model and two partial covering absorbers.

3.5. *PQ Gem*

PQ Gem was the first IP found to have a soft-X-ray component (Mason et al. 1992). This component was also present in the *XMM* data, with a best-fitting blackbody temperature of $47.6^{+2.9}_{-1.4}$ eV, in agreement with the 46^{+12}_{-23} eV of Duck et al. (1994) from *ROSAT* data, and 56^{+12}_{-14} eV of de Martino et al. (2004) from *BeppoSAX* data. The fitted column density goes to zero, which is likely to be an artefact of fitting a complex absorption with too simple a model. We quote an upper limit of 3×10^{19} cm^{-2} based on the phase-resolved modelling of Evans et al. (2006).

3.6. *EX Hya*

The best-fitting model for EX Hya used a blackbody component, which has not been previously reported in this system. However even with this component, the procedure outlined in Section 2 resulted in a poor fit (χ^2_ν=2.1). A possible reason for this is our choice of absorption model. We have used a cold absorber in our models since the data do not warrant the extra parameters in ionised absorption models, even though one expects any absorbing material (e.g. the accretion curtains) to be ionised. We therefore tried various ionised absorption models, but gained only a minor improvement to the fit. We thus reverted to the cold absorber model for consistency with the rest of this paper. We also tried using phase-resolved spectroscopy, in case the poor fit was the result of averaging phase-variant parameters, however this still did not yield an acceptable fit. We have nonethless included our results for EX Hya, for completeness, but due to the poor fit, we do not much place much weight on the EX Hya data when considering our results.

As the distance to EX Hya is known (64.5±1.2 pc: Beuermann et al. (2003)), we can determine the size of the accretion footprint from the soft X-ray flux. Table 4 gives this as $(1.59^{+3.47}_{-0.62}) \times 10^{-10}$ ergs cm^{-2} s^{-1} with a temperature of $31.0^{+1.3}_{-2.4}$ eV, from which we compute an emitting area $(8.4^{+29.8}_{-4.2}) \times 10^{13}$ cm^2. Suleimanov et al (2005) gave the mass of the white dwarf in EX Hya as $0.5 \pm 0.05\, M_\odot$, thus the observed blackbody emitting area in EX Hya covers $(7.3^{+29.3}_{-4.0}) \times 10^{-4}$ of the white-dwarf surface.

3.7. *UU Col*

UU Col was identified as a soft IP by Burwitz et al. (1996). de Martino et al. (2006) have recently confirmed this with a detailed analysis of the *XMM* observation. They reported a blackbody temperature of $49.7^{+5.6}_{-2.9}$ eV, which is lower than our value of 73^{+20}_{-9} eV, however in their model the blackbody is absorbed by the partial covering absorber, and no simple absorber is present.

3.8. *WX Pyx*

The XMM observation of WX Pyx, the only X-ray observation of this star to date, has a relatively low statistical quality. It was previously analysed by Schlegel (2005) who did not report looking for a blackbody component. However, we find that adding a blackbody does significantly improve the fit.

3.9. *Comparison with the polars*

In Fig. 2 we have plotted the softness ratios of both the IPs and the polars (from RC04). For the polars which RC04 reported not to have a blackbody, we obtained the spectra as extracted an calibrated by RC04 (Ramsay, private communication), and fitted them in the same way as the IPs (Section 2) to obtain an upper limit.

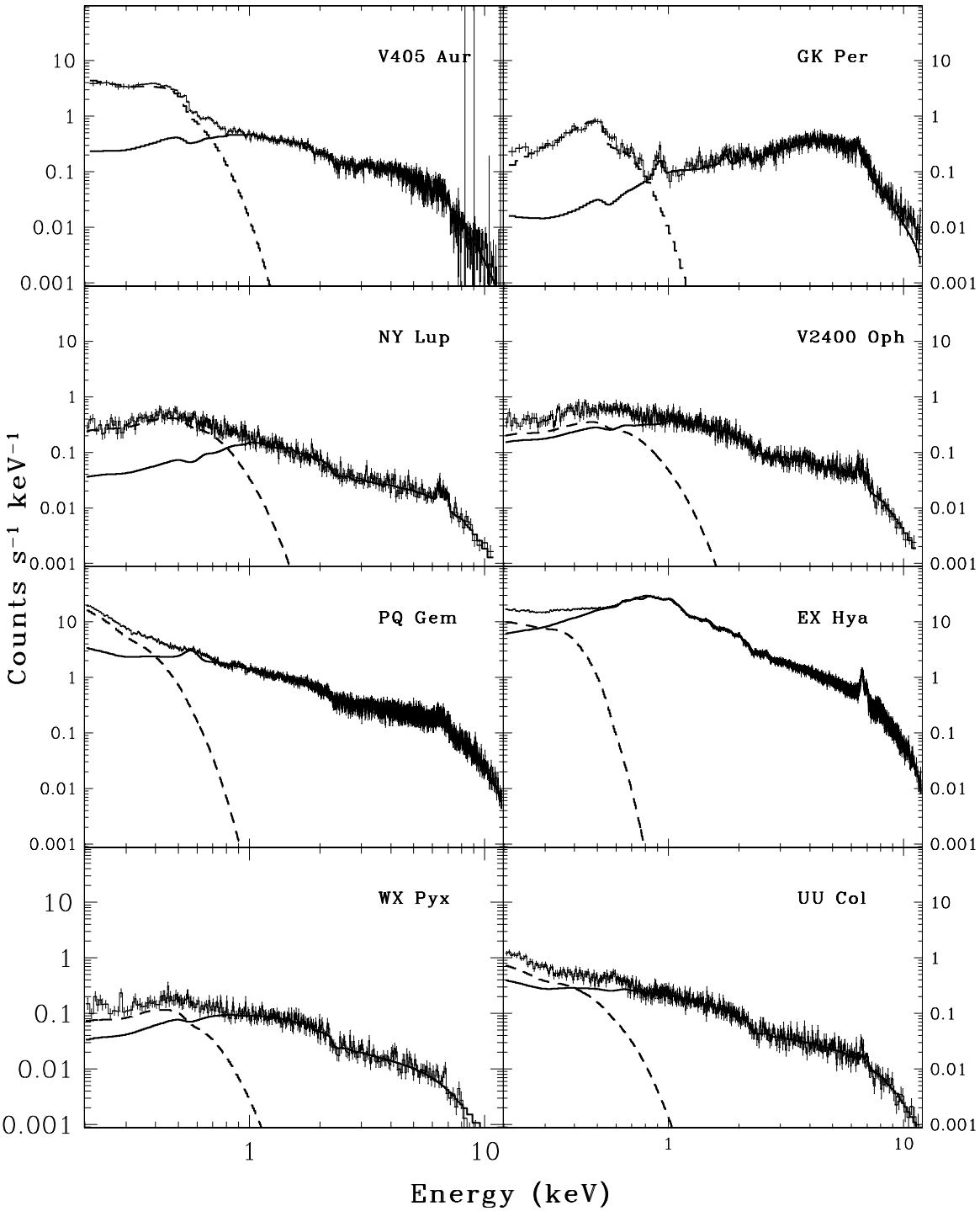

FIG. 3.— The EPIC-pn spectra of the eight IPs for which the best-fitting models contain a blackbody component. The solid line shows the hard component; the broken line the blackbody. For V405 Aur we have shown the MOS-1 spectrum, since the pn camera did not collect any data.

The chief difference in the two distributions is that while several polars show a softness ratio > 0.5, no IP can be confirmed to do this, and it can be excluded for all but EX Hya – for which our results are uncertain (Section 3.6). The 'soft excess' in polars is believed to arise due to 'blobby accretion' (e.g. Kuijpers & Pringle (1982)). In this model, dense blobs of matter penetrate into the white dwarf photosphere and the energy is thermalised to a blackbody.

Whether such accretion occurs in IPs has not been widely discussed in the literature. Hellier & Beardmore (2002) suggested that viscous interactions in an accretion disc would destroy blobs, although Vrielmann et al. (2005) interpreted flares in the lightcurve of GK Per as resulting from the accretion of blobs. Our findings suggest that blobby accretion is not significant in IPs.

4. DISCUSSION

The 'polar' class of magnetic cataclysmic variable has long been known to be characterised by a soft blackbody component (e.g. King & Watson (1987)). This

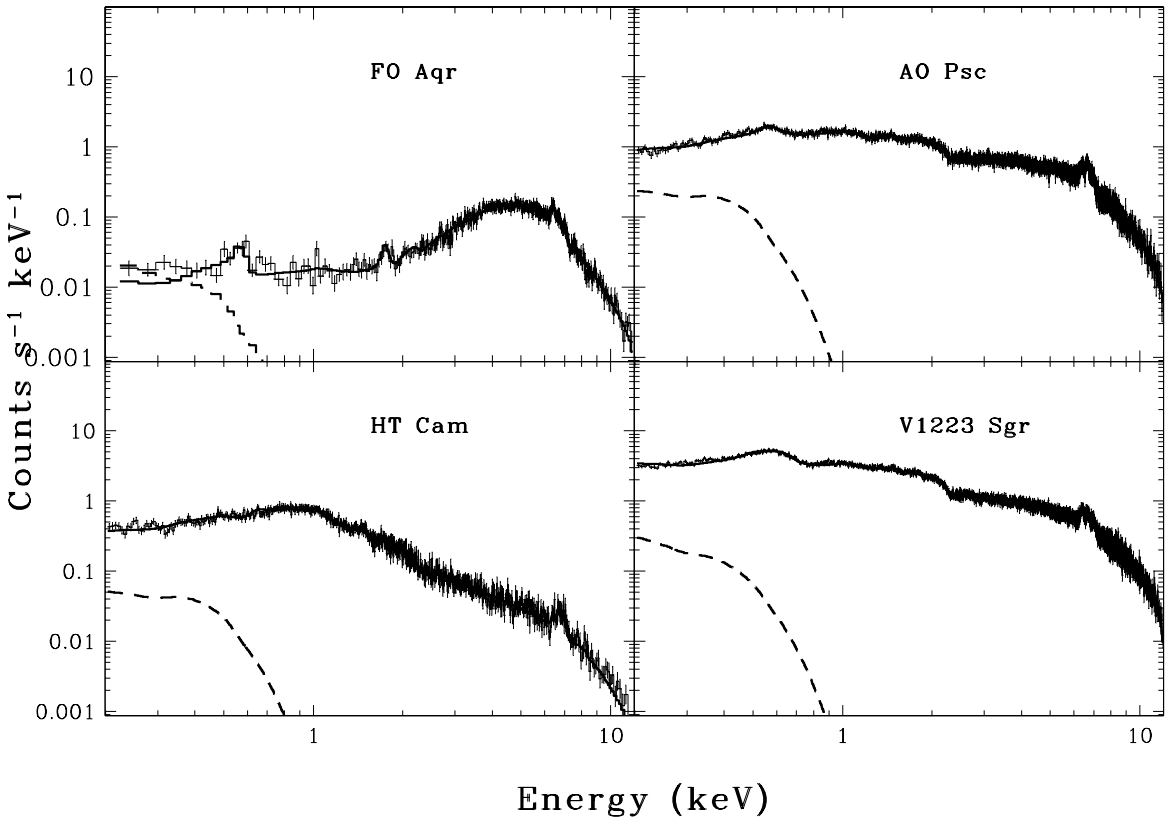

FIG. 4.— The EPIC-pn spectra of the four IPs for which the best-fitting model does not contain a blackbody component. The solid line shows the best-fitting model. The broken line shows the upper limit to a blackbody component, given a temperature of 60 eV. For FO Aqr we show the MOS-1 data, as the signal-to-noise ratio of the pn data is worse.

is considered to arise from the white-dwarf surface, heated either by reprocessing of hard X-rays from the accretion column, or by thermalisation of blobs of accretion (e.g. Kuijpers & Pringle (1982)). In contrast, IPs were thought to lack this component (e.g. King & Lasota (1990)). However, observations with *ROSAT* found a blackbody component in some IPs, leading Haberl & Motch (1995) to suggest that there were two spectrally distinct classes of IP. This raised the question of why.

To address this we have conducted a systematic survey of the spectral characteristics of the IPs observed with *XMM-Newton*, which has much greater spectral coverage and throughput than *ROSAT*.

We find that, of twelve IPs analysed, eight show a soft blackbody component while four do not. This suggests that a blackbody is a normal component of IPs, and hence of accretion onto magnetic white dwarfs, and that the spectra differ only in degree.

We thus ask what causes the differing visibility of the soft component. There does not appear to be any correlation with the white-dwarf mass [see Cropper et al. (1999); Ezuka & Ishida (1999); Ramsay (2000); Suleimanov et al (2005) for mass estimates], nor any obvious correlation with the orbital period.

In polars, systems with higher magnetic field strengths appear to have higher softness ratios (e.g. Ramsay et al. (1994)). Of the IPs in our sample showing polarisation, and thus known to have a relatively strong field (5–20 MG), all (PQ Gem, V405 Aur and V2400 Oph) show a blackbody component, while the four stars showing no blackbody emission (FO Aqr, AO Psc, HT Cam & V1223 Sgr) do not show polarisation. We give a possible explanation for this after discussing the role of absorption.

We first consider the simple absorber, which is probably of interstellar origin. The detection of a blackbody component in most systems shows that interstellar absorption is not sufficient to extinguish the soft emission. Further, the systems with no detected blackbody component do not have higher interstellar columns than those with a blackbody (Table 3), so this absorption cannot explain the differing visibility of the soft component.

We thus turn to the partial-covering absorption, which in IPs is predominantly caused by the accretion curtains crossing the line of sight. Here we find that the systems where the lightcurves are dominated by deep absorption dips owing to the accretion curtains (FO Aqr, V1223 Sgr and AO Psc; see Beardmore et al. (1998); Beardmore et al (2000); Hellier et al. (1991) respectively) do tend to be those which lack a blackbody component. In contrast, systems showing a blackbody component, such as V405 Aur, NY Lup, EX Hya and V2400 Oph, tend to be systems where the lightcurves suggest that the accretion curtains do not hide the accretion footprints (see Evans & Hellier (2004); Haberl et al. (2002); Allan et al. (1998); Hellier & Beardmore (2002) respectively).

We thus suggest that the major reason why some IPs don't show a blackbody component is simply that the heated region near the accretion footprint is hidden by the accretion curtains, while in other IPs it is not, the difference being the result of the system inclination and the magnetic colatitude (see Fig. 5). Coupled with this is

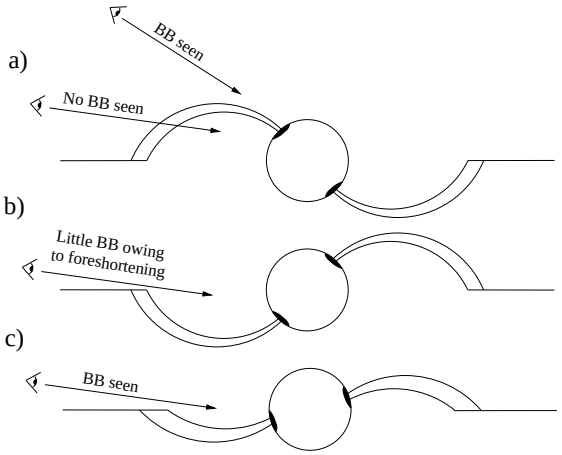

FIG. 5.— The factors that affect blackbody emission in an IP.
a) When the upper magnetic pole is on the visible face, blackbody emission will only be seen if the inclination is such that the heated accretion region is visible above the accretion curtains.
b) When the lower pole is on the visible face, it will likely be too foreshortened for us to detect blackbody emission.
c) In UU Col the magnetic axis is highly inclined, so the foreshortening seen in b) is reduced and blackbody emission is seen.

the effect of foreshortening, such that an optically thick heated region will not produce much blackbody emission if it is only seen while on the white-dwarf limb, rather than in the middle of the face.

A proper investigation of this idea would need knowledge of the size and location of the accretion footprints and of the surrounding heated polecaps, so that we could estimate the difference absorbing columns of different spectral components, and how these vary with spin-cycle phase. However, this information is not known for the majority of IPs. The softness ratio might conceivably also vary with parameters such as accretion rate and white-dwarf mass, which are again only poorly known.

However, as a test of our ideas, we can outline how they might apply to the remaining systems in our sample which we did not consider when forming the model, namely HT Cam, GK Per, PQ Gem and UU Col.

In PQ Gem the accretion curtains do cause an absorption dip when they obscure the accretion footprints. However, the geometry of this star is relatively well determined (Potter et al. 1997; Mason 1997; Evans et al. 2006) and it appears that the heated polecap is grazingly visible above the accretion curtain for part of the cycle; thus it shows both an absorption dip and a soft blackbody, and is on the boundary between the two cases illustrated in the upper panel of Fig. 5.

UU Col also shows an absorption dip when the accretion curtains obscure the upper pole, and also shows blackbody emission. de Martino et al. (2006) proposed that the blackbody emission comes from the lower pole, viewed when that pole is closest to us (lowest panel of Fig. 5). We thus suggest that UU Col has an abnormally high inclination of the magnetic dipole, such that the lower pole is not foreshortened as much as in other IPs where no blackbody component is seen. V405 Aur is another system that appears to have a highly inclined dipole, such that blackbody emission from the lower pole is significant, leading in that system to a double-peaked soft-X-ray lightcurve (Evans & Hellier 2004).

In contrast to all the other IPs, the *XMM* data of GK Per reported here were collected during an outburst.

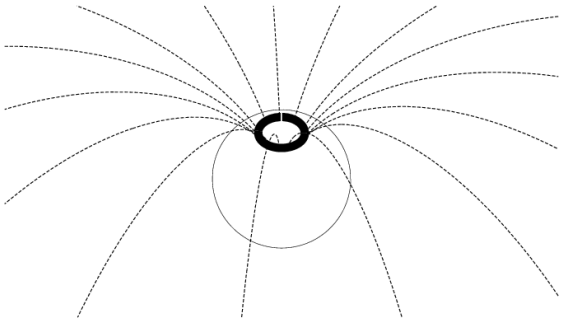

FIG. 6.— Schematic diagram of GK Per in outburst. Accretion occurs from all azimuths, resulting in a circular blackbody-emitting region (dark ring). As can be seen, even when the accretion curtains lie across our line-of-sight, part of this region is unobscured.

Hellier et al. (2004) have argued that during outburst the accretion occurs from all azimuths, forming a complete accretion ring at the poles. As illustrated in Fig. 6, this means that some portion of the heated polecap is likely to be visible 'behind' the magnetic pole, where accretion does not normally occur. Thus in GK Per in outburst we see a system with both strongly absorbed X-ray emission (from in front of the magnetic pole) and a blackbody component.

Lastly, we consider HT Cam. This shows very little sign of absorption, and its lightcurve can explained without any absorption effects (Evans et al. 2006). Yet it shows no blackbody emission, in apparent contradiction to our model. However, as previously suggested by de Martino et al. (2006) and Evans et al. (2006), it appears that HT Cam has an exceptionally low accretion rate (partly accounting for the lack of absorption). If so, it could be that the blackbody component is simply too cool to be detected in the *XMM* bandpass. We note that the blackbody temperature in EX Hya, the other star in our sample below the period gap, is lower than in the others (Table 3), and that in HT Cam might be lower still.

5. SUMMARY

We have analysed data from *XMM* observations of 12 intermediate polars and find that a soft blackbody component is a common feature of their X-ray spectra. We suggest that in the systems showing no blackbody emission the heated accretion polecaps are largely hidden by the accretion curtains, or are only visible when on the white dwarf limb and highly foreshortened. Thus IPs with lightcurves dominated by absorption dips caused by the passage of accretion curtains across the line of sight tend to show no blackbody emission. Further, these are also the systems least likely to show polarisation, since the cyclotron-emitting column will also be obscured by the accretion curtains, or would be beamed away from us if the accretion region were on the white-dwarf limb. After comparing the blackbody emission seen in IPs with that seen in polars, we conclude that the blobby emission responsible for soft X-ray excesses in polars does not occur in IPs.

ACKNOWLEDGEMENTS

We thank Gavin Ramsay for providing us with the spectra of the polars with no detectable soft component.

Facilities: XMM ()

REFERENCES

Allan, A., Hellier, C., Beardmore, A. 1998, MNRAS, 295, 167
Beardmore, A.P., Mukai, K., Norton, A.J., Osborne, J.P., Hellier, C. 1998, MNRAS, 297, 337
Beardmore, A.P., Osborne, J.P., Hellier, C. 2000, MNRAS, 315, 307
Beuermann, K., Harrison, Th.E., McArthur, B.E., Benedict, G.F., Gänsicke, B.T. 2003, A&A, 412, 821
Beuermann, K., Harrison, Th.E., McArthur, B.E., Benedict, G.F., Gänsicke, B.T. 2004, A&A, 419, 291
Burwitz, V., Reinsch, K., Beuermann, K., Thomas, H.-C. 1996, MNRAS, 310, L25
Cropper, M., Wu, K., Ramsay, G., Kocabiyik, A. 1999, MNRAS, 306, 684
Cropper, M., Ramsay, G., Hellier, C., Mukai, K., Mauche, C., Pandel, D. 2002, SPTA, 360, 1951
de Martino, D., Matt, G., Belloni, T., Haberl, F., Mukai, K. 2004, A&A, 415, 1009
de Martino, D. et al. 2005, A&A, 437, 935
de Martino, D., Matt, G., Mukai, K., Bonnet-Bidaud, J.-M., Burwitz, V., Gänsicke, B.T., Haberl, F., Mouchet, M. 2006, A&A, 454, 287
den Herder, J.W., et al. 2001, A&A, 365, 7
Duck, S.R., Rosen, S.R., Ponman, T.J., Norton, A.J., Watson, M.G., Mason, K.O. 1994, MNRAS, 271, 372
Evans, P.A., Hellier, C. 2004, MNRAS, 353, 447
Evans, P.A., Hellier, C. 2005a, MNRAS, 359, 1531
Evans, P.A., Hellier, C. 2005b, in Hameury, J.M., Lasota, J.P., eds., ASP Conf. Ser. Vol. 330, The astrophysics of cataclysmic variables and related objects, Astron. Soc. Pac., San Francisco, p. 165
Evans, P.A., Hellier, C., Ramsay, G., Cropper, M. 2004, MNRAS, 349, 715
Evans, P.A., Hellier, C., Ramsay, G. 2006, MNRAS, 369,1229
Evans, P.A., Hellier, C., Ramsay, G., Cropper, M. 2007, in preparation
Ezuka, H., Ishida, M. 1999, ApJ, 120, 277
Frank, J., King, A.R., Raine, D.J. 2002, Accretion Power in Astrophysics, 3rd ed., Cambridge University Press, Cambridge, UK
Haberl, F., Motch, C. 1995, A&A, 297, L37
Haberl, F., Thorstensen, J.R., Motch, C., Schwarzenberg-Czerny, A., Pakull, M, Shambrook, A., Pietsch, W., 1994, A&A, 291, 171
Haberl, F., Motch, C., Zickgraf, F.-J. 2002, A&A, 387, 201
Hellier, C. 2001, Cataclysmic Variable Stars, Springer-Praxis, Chichester, UK
Hellier, C., Beardmore, A.P. 2002, MNRAS, 331, 407
Hellier, C., Cropper, M., Mason, K.O. 1991, MNRAS, 249, 235
Hellier, C., Mukai, K., Ishida, M., Fujimoto, R. 1996, MNRAS, 280, 877
Hellier, C., Harmer, S., Beardmore, A.P. 2004, MNRAS, 349, 710
Ishida, M., Sakao, T., Makishima, K., Ohashi, T., Watson, M.G., Norton, A.J., Kawada, M., Koyama, K. 1992, MNRAS, 254, 647
James, C.H., Ramsay G., Cropper, M., Branduardi-Raymont, G. 2002, MNRAS, 336, 550
Jansen F. et al., 2001, A&A, L1
King, A.R., Watson, M.G. 1987, MNRAS, 227, 205
King, A.R., Lasota, J.P. 1990, MNRAS, 247, 214
Kuijpers, J., Pringle, J.E. 1982, A&A, 114, 4
Mason, K.O. 1997, MNRAS, 285, 493
Mason, K.O. et al., 1992, MNRAS, 258, 749
Mukai, K., Kinkhabwala, A., Peterson, J.R., Kahn, S.M., Paerels, F. 2003, ApJ, 586, L77
Norton, A.J., Watson, M.G., King, A.R., Lehto, H.J., McHardy, I.M. 1992, MNRAS, 254, 705
Patterson, J. 1994, PASP, 106, 209
Potter, S.B., Cropper, M., Mason, K.O., Hough, J.H., Bailey, J.A. 1997, MNRAS, 285, 82
A. 2002,
Ramsay, G., Mason, K.O., Cropper, M., Watson, M.G., Clayton, K.L. 1994, MNRAS, 270, 692
Ramsay, G. 2000, MNRAS, 314, 403
Ramsay, G., Cropper, M. 2004, MNRAS, 347, 497 (RC04)
Schlegel, E.M. 2005, A&A, 433, 635
Staude, A., Schwope, A.D., Krumpe, M., Hambaryan, V., Schwarz, R. 2003, A&A, 406, 253
Strüder, L., et al. 2001, A&A, 365, 18
Suleimanov, V., Revnivtsev, M., Ritter, H. 2005, A&A, 435, 191
Turner, M.J.L., et al. 2001, A&A, 365, 27
Vrielmann, S., Ness, J.-U., Schmitt, J.H.M.M. 2005, A&A, 439, 287
Warner, B. 1987, MNRAS, 227, 23
Warner, B. 1995, Cataclysmic Variable Stars, Cambridge University Press, Cambridge, UK
Watson, M.G., King, A.R., Osborne, J. 1985, 212, 917